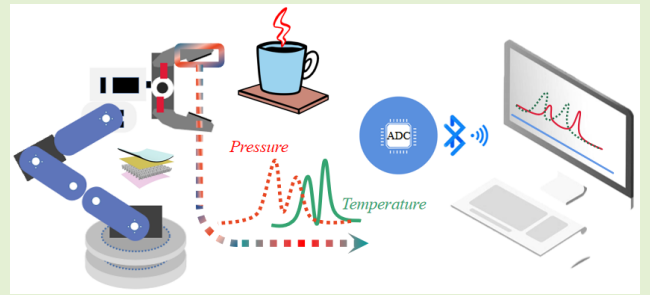


A Vertically Stacked Dual-Parameter Sensor for Simultaneous Temperature and Pressure Detection

Shiqi Chen, Xiaolong Han, Faxin Zhong, Xiangyu Yin[✉], Yue Zhang[✉], and Bingwei He[✉]

Abstract—The ability of electronic skin to detect and distinguish multiple tactile stimuli is important to properly mimic human skin. Although a few dual-parameter sensors have recently been designed to identify the most common tactile stimuli such as pressure and heat, it remains a difficult task to develop a dual-parameter sensor that is free from signal interference, easy to prepare, and signal readout, and requires no bias voltage. Here, we develop a simple but effective vertical stacking of sensing components strategy for high-performance dual-parameter sensing systems, in which multiwalled carbon nanotubes (MWCNTs)/textile and PEDOT:PSS/photopaper were designed as pressure- and thermal-sensitive components, and a layer of double-sided tape with a thickness of 200 μm is sandwiched between two sensitive components for electrical and thermal isolation. The dual-parameter sensor exhibits good sensing performance in terms of sensitivity, response time, detection range, and stability for both pressure and temperature detection. More importantly, the tactile inputs of pressure and temperature can be distinguished without signal decoupling. The preparation of the dual-parameter sensor is simple and low cost, and its requirements for the readout device are as low as a single-chip microcomputer. This work provides a promising prototype for multiparameters e-skin, which has great potential for applications in robot applications, human–computer interaction, and intelligent wearable devices.



Index Terms—Bionic electronic skin, dual-parameter, signal decoupling, tactile perception.

I. INTRODUCTION

BIONIC electronic skin is increasingly used in the field of robotics and human–computer interaction benefiting from its conformal deformation and tactile perception function similar to human skin [1], [2], [3]. The ability of human skin in simultaneously perceiving and distinguishing various external stimuli (e.g., pressure, strain, pain, and temperature) should be attributed to the presence of vari-

ous sensory receptors, namely, mechanoreceptors, thermoreceptors, nociceptors, and chemoreceptors that are embedded at different depths inside soft tissue, and each class of receptors is specifically designed to perceive specific stimuli and transmit the corresponding nerve impulses to the brain [4]. Therefore, to make the electronic skin better mimic the perceptual characteristics of human skin, it should have the ability to detect and distinguish multiple tactile stimuli.

Pressure and thermal are the most common tactile stimuli in life, so to properly mimic human skin, successful discrimination between the two stimuli becomes very important. Dual-parameter sensing systems are typically obtained by integrating thermal and pressure-sensitive components in-plane or out-of-plane into a sensing platform [5], [6], [7], in which each sensor outputs an electrical signal targeting a specific tactile stimulus. However, the output signals of these two stimuli are usually measured by a single electrical readout device, and due to the coupling between the output signals, a combined signal pattern is usually presented, which complicates the discrimination between the tactile inputs. A common strategy to overcome this limitation is to develop a dual-parameter sensor in which one sensing unit is insensitive to the other tactile input [8]. Since the capacitance sensor is by nature insensitive to temperature, the pressure-sensitive units in a dual-parameter sensing system are often designed based

Manuscript received 26 December 2022; revised 27 January 2023; accepted 30 January 2023. Date of publication 7 February 2023; date of current version 14 March 2023. This work was supported in part by the National Natural Science Foundation of China under Grant 52103025 and in part by the Natural Science Foundation of Fujian Province of China under Grant 2021J01644. The associate editor coordinating the review of this article and approving it for publication was Prof. Mehdi Javamard. (*Shiqi Chen and Xiaolong Han contributed equally to this work.*) (*Corresponding authors:* Xiangyu Yin; Yue Zhang; Bingwei He.)

Shiqi Chen, Faxin Zhong, Yue Zhang, and Bingwei He are with the College of Mechanical Engineering and Automation, Fuzhou University, Fuzhou 350108, China (e-mail: 210220045@fzu.edu.cn; 210220052@fzu.edu.cn; yuezhang@fzu.edu.cn; mybwhe@fzu.edu.cn).

Xiaolong Han is with the College of Maynooth International Engineering Collage, Fuzhou University, Fuzhou 350108, China (e-mail: 831902106@fzu.edu.cn).

Xiangyu Yin is with the College of Chemical Engineering, Fuzhou University, Fuzhou 350108, China (e-mail: xyin65@fzu.edu.cn).

This article has supplementary downloadable material available at <https://doi.org/10.1109/JSEN.2023.3241794>, provided by the authors.

Digital Object Identifier 10.1109/JSEN.2023.3241794

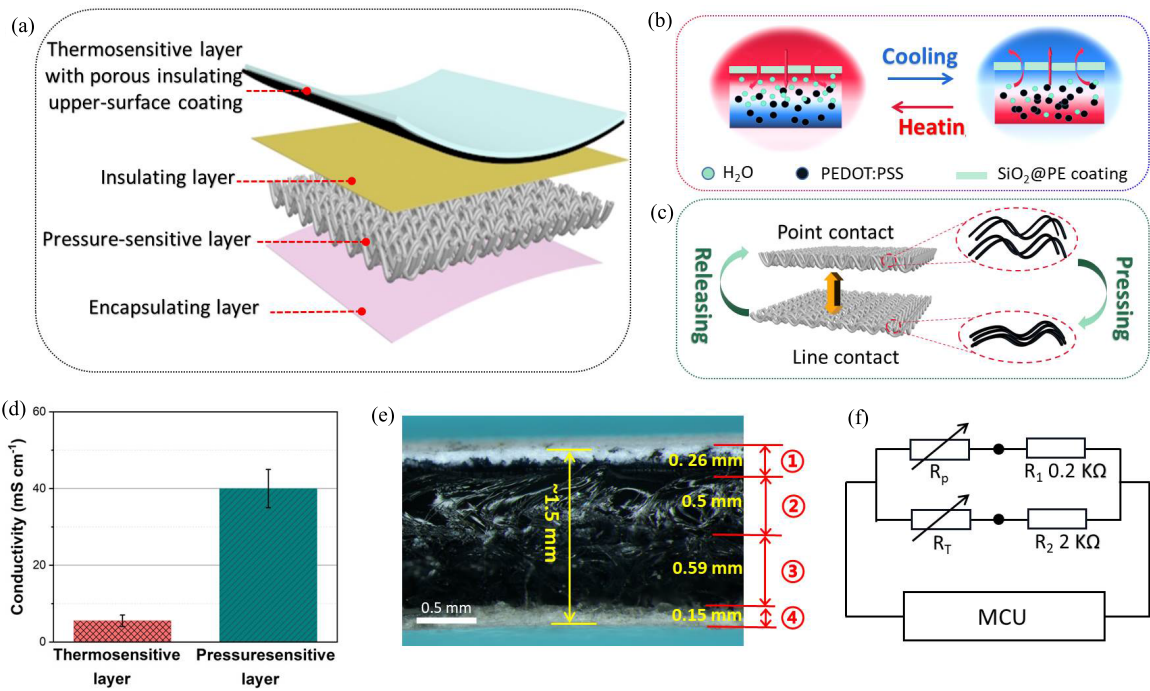


Fig. 1. Design and fabrication of the VSDPS. (a) Schematic illustrating the structure of the VSDPS. Schematic illustrating the working mechanism of (b) temperature and (c) pressure sensing. (d) Conductivity of the thermosensitive layer and the pressure-sensitive layer. (e) Cross-sectional optical image showing the multilayer structure of the VSDPS. ①–④ are the thermosensitive layer with microporous, insulating $\text{SiO}_2@\text{PE}$ coating, the insulating layer of 3M double-sided tape, the pressure-sensitive layer, and the encapsulating layer of 3M single-sided tape, respectively. (f) Circuit diagram of the device consisting of R_p and R_T connected in parallel. R_p and R_T are the variable resistance for pressure sensing and temperature sensing, respectively. R_1 and R_2 are the fixed value resistors for modulating circuit. MCU is the microcontroller unit.

on capacitive sensing mechanism [4], [9], [10], [11]. In this way, the tactile inputs can be decoupled by first analyzing the pressure signal and then analyzing their combined signal patterns. However, to reduce the crosstalk between each tactile sensing unit as well as to improve the sensitivity of capacitive pressure units, special microstructure design is often necessary, which makes the preparation process of this type of dual-parameter sensors, particularly sophisticated and difficult to manufacture. In contrast, the fabrication of another type of dual-parameter sensors with a sandwich structure is much simpler, in which the sandwiched active material, obtained by combining thermoelectric materials with porous elastomer, can react to both temperature and pressure based on piezoresistive and thermoelectric effects [12], [13]. Since piezoresistive and thermoelectric effects result in different IV characteristics (the voltage shift targets the temperature, while the slope of the resistive behavior is related to the pressure) in a single current–voltage (I – V) curve, pressure and temperature could be distinguished without additional signal decoupling. However, thermoelectric sensors tend to be less sensitive to temperature changes and have less material selectivity than thermosensitive sensors [14], [15]. More troublesome is that such sensors often require a certain bias voltage applied by an external power supply to achieve tactile stimuli detection [16]. To solve this trouble, Shin et al. [17] developed a triboelectric nanogenerator-based dual-parameter temperature–pressure sensor, in which the ferroelectric polymer of P(VDF-TrFE) with its counter electrode served as the identical contact pair materials, and by switching the triboelectric polarity via ferroelectric polarization, pressure and temperature could be

discriminated based on the triboelectric and pyroelectric effect. However, the output signal change of this sensing platform to pressure input is very tiny (in the order of 10^{-9} A), which puts forward high requirements for the accuracy of the signal readout device. Therefore, it is necessary to develop a new approach of multimodal sensor that can distinguish between pressures and temperature without signal interference and has characteristics of easy to readout, no bias voltage required, and facile to prepare.

Here, we develop a simple but effective vertical stacking of sensing components strategy for high-performance dual-parameter sensing systems, in which multiwalled carbon nanotubes (MWCNTs)/textile and PEDOT:PSS/photopaper were designed as pressure- and thermal-sensitive components, and a layer of double-sided tape is sandwiched between two sensitive components for electrical and thermal isolation. Although both sensitive components measure tactile inputs based on resistance changes, the temperature output is insensitive to pressure input, and the pressure output signal is less susceptible to interference from temperature input due to the presence of thermal insulation. Thus, the tactile inputs of pressure and temperature can be distinguished without signal decoupling by our developed vertically stacked dual-parameter sensor (referred to as VSDPS). The preparation of VSDPS is simple and low cost, and its requirements for the readout device are as low as a single-chip microcomputer can complete the accurate detection and distinguish. Besides, the VSDPS exhibits good sensing performance in terms of sensitivity, response time, detection range, and stability for both pressure and temperature detection, as bionic electronic

skin, the VSDPS presents great application potential in robot applications, human-computer interaction, and intelligent wearable devices.

II. RESULTS AND DISCUSSION

A. Operation Principle and Design of the VSDPS

Based on the resistive sensing principle, we design a class of prototypical tactile-sensitive VSDPS devices to simultaneously detect and discriminate temperature and pressure. As shown in Fig. 1(a), the VSDPS composed of four layers, namely, a sandwiched insulating layer, a pressure-sensitive layer, a thermosensitive layer distributed on the upper and lower surfaces of the insulating layer, and an encapsulating layer covering the pressure-sensitive layer. We used a commercially available resin-coated photopaper as the flexible substrate for thermosensitive sensor fabrication, which sandwiched an ink-fixing layer between top microporous $\text{SiO}_2@\text{PE}$ coating and bottom cellulose base paper (see Fig. S1(a)–(c) in the Supporting Information). In the sensors' preparation process, the PEDOT:PSS thermosensitive ink was first dropped from the cellulose base paper side onto the above flexible substrate by an inkjet dispensing technology, and then, the ink was quickly absorbed, filled the gaps between cellulose fibers, and diffused spontaneously to the mid-ink-fixing layer (see Fig. S2 and S3(a) in the Supporting Information). By adjusting the ink droplet and the printing speed, the ink can be controlled to only stay in the ink-fixing layer and not continue to diffuse downward, and through the microporous $\text{SiO}_2@\text{PE}$ coating, evidenced by no S element can be detected on the $\text{SiO}_2@\text{PE}$ coating after dispensing (see Fig. S3(b) and (c) in the Supporting Information). In this way, the top surface of the thermosensitive sensor acted by the microporous $\text{SiO}_2@\text{PE}$ coating is electrically insulating, and the thermosensitive ink can be firmly locked under it, making the sensor's response to temperature stable and durable. More importantly, the microporous structure of the top coating is conducive to the rapid exchange of heat to improve the sensitivity and responsiveness of the sensor. The above characteristics indicate that the resin-coated photopaper-based flexible temperature sensor can show a good overall performance without additional encapsulation layer. It is well known that the conductivity of the PEDOT:PSS depends on the network characteristics of the complex [18], [19], [20] and intermolecular water content. When an object with a higher temperature approaches the thermosensitive sensor, the heat will rapidly diffuse to the underlying thermosensitive layer through the microporous structure of the surface $\text{SiO}_2@\text{PE}$ coating so that the intermolecular water in the PEDOT:PSS network is heated, evaporated, and even gathered to the junction of the ink-fixing layer and the $\text{SiO}_2@\text{PE}$ coating [see Fig. 1(b)]. Naturally, the intermolecular water content is likely to decrease, which will increase the adhesion between the molecules in the PEDOT:PSS network, thereby increasing the conductivity. Next, when an object with a low temperature approaches the thermosensitive sensor or the sensor is placed in a lower temperature environment, the heat inside the sensor will also rapidly diffuse into the air through the microporous structure of the surface $\text{SiO}_2@\text{PE}$ coating. At this time, the intermolecular water molecules will migrate back to their original positions, and the resistance

of the thermosensitive layer will return to the initial value. In addition, we also tried to use inkjet printing technology to prepare thermosensitive layers with designed patterns, but the results were not satisfactory. On the one hand, the water absorption capacity of paper-based materials is so great that it is difficult to control the printing parameters for fine pattern preparation (see Fig. S4 in the Supporting Information). On the other hand, inkjet printing is very time-consuming. It should take 25 min to prepare a single thermosensitive layer with a size of $5 \times 10 \text{ mm}^2$, while it only takes less than 10 s to prepare a thermosensitive layer with the same conductivity and the same size using the inkjet dispensing technology. Obviously, the inkjet dispensing technology is more convenient and conducive to mass production (see Fig. S5 in the Supporting Information).

Meanwhile, the pressure-sensitive layer was fabricated by using a double-knit, dust-free wipe as the flexible substrate. Through a simple dipping-drying procedure, the conductive MWCNTs were uniformly attached to each fabric fiber as shown in Fig. S6 in supporting information, and a flexible MWCNTs/fabric pressure sensing layer could be obtained. No doubt the double-knit fabric structure of the wipe imparts softness, compressibility, and elasticity to the pressure-sensitive layer. Fig. 1(c) shows the natural contact between the knit loops in the cross section of the pressure-sensitive layer. Obviously, point contact is the main contact model between knit loops, and there are many gaps between the contact points that provide space for the knit loops to deform under pressure. Specifically, when a vertical pressure is applied to the sensitive layer, the contact points of the knit loops of the fabric will increase, resulting in a larger total contact area, and therefore, the resistance of the pressure-sensitive layer decreases. When the pressure is subsequently released, the knit loops restore to the initial contact state, so the resistance of the entire pressure-sensitive layer returns to its original value. We used five thermal layers and five pressure-sensitive layers as test samples, and the initial resistance of each sample was measured five times to estimate the initial conductivity of this layer. The initial conductivity of the optimized thermosensitive layer and the optimized pressure-sensitive layer is 5.6 ± 0.6 and $40.1 \pm 0.5 \text{ mS cm}^{-1}$, respectively [see Fig. 1(d)].

Next, a piece of 3M double-sided tape with a thickness of 0.5 mm was sandwiched between the thermosensitive layer and the pressure-sensitive layer [see Fig. 1(e)]. The purpose of using such thick tape as an insulating layer is twofold. On the one hand, it is to prevent electric leakage between the upper and lower sensitive layers to ensure the accuracy of the measured data. On the other hand, the thick insulating layer can prevent the temperature of the object to be measured from being transmitted to the pressure-sensitive layer on its lower surface. As shown in Fig. S7 in the Supporting Information, when a 65°C object touched the top surface of the double-sided tape, the top surface rapidly heated up to 65°C , while the temperature of the bottom surface increased by less than 10°C , demonstrating its role in reducing the influence of temperature on the response signal of the pressure-sensitive component, and thus realized crosstalk-free dual-parameter tactile stimulation detection. Also, an extra layer of 3M single-sided

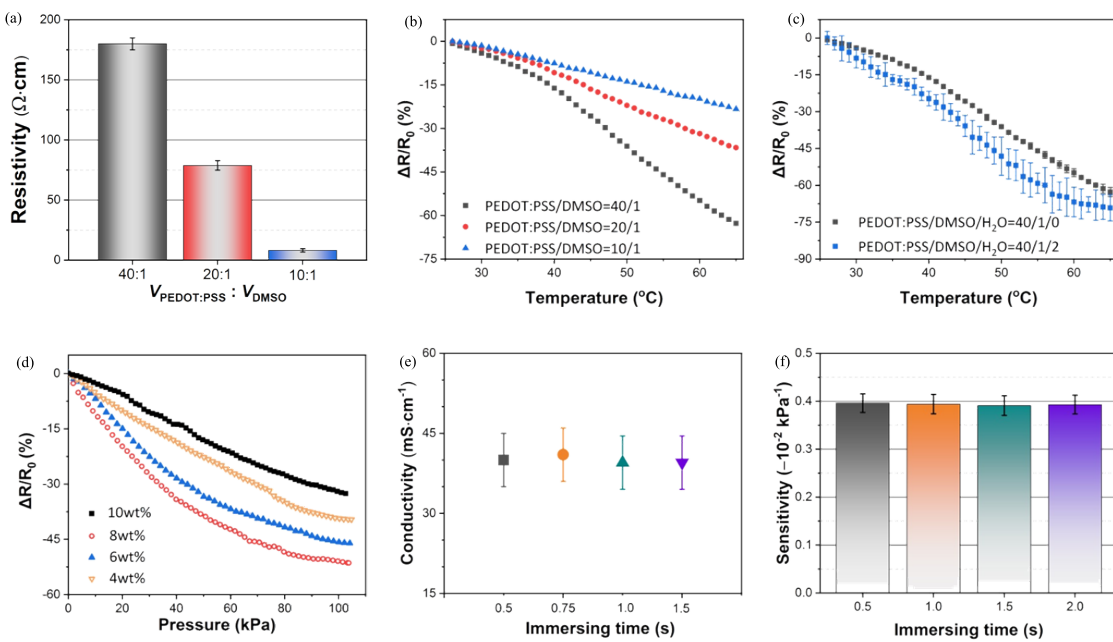


Fig. 2. Characterization and optimization of the temperature sensors and the pressure sensors. Effects of DMSO content on (a) resistivity and (b) sensitivity of the thermosensitive layer. (c) Effect of H₂O content on the sensitivity of the thermosensitive layer. (d) Effect of concentration of the MWCNTs water dispersion on the sensitivity of the pressure-sensitive layer. Effects of immersing time on (e) initial conductivity and (f) sensitivity of the pressure-sensitive layer.

tape (~0.15 mm) was attached to the other surface of the pressure-sensitive layer for insulating and sealing. To this point, a touch-sensitive device with dual modes of temperature and pressure sensing has been fabricated. The overall thickness of the dual-parameter sensor is less than 1.5 mm, of which the thermosensitive layer is about 54 μm (see Fig. S2) and the pressure-sensitive layer is about 0.59 mm. Although the VSDPS is thicker than single-parameter flexible sensors, it is thinner than most dual-parameter sensors [12], [13], [16], which makes it more promising application potential in human-computer interaction, robotics, health detection, and other fields. An equivalent circuit diagram for the VSDPS-based sensing system is shown in Fig. 1(f), in which R_p and R_t are the variable resistance for pressure sensing and temperature sensing, respectively.

B. Performance Improvement of the Temperature Sensor and the Pressure Sensor

Because the conductivity of the PEDOT:PSS depends on the network characteristics of the complex [21], [22], [23], [24] and intermolecular water content, we have first studied the effects of dimethyl sulfoxide (DMSO) and water on the conductivity and sensitivity of the thermosensitive layer by measuring the initial resistance (five test samples were taken for each ratio of PEDOT:PSS and DMSO). Fig. 2(a) shows that when the volume ratio of PEDOT:PSS and DMSO is 40:1, 20:1, and 10:1, the initial resistance of the thermosensitive layer is 179.98 ± 5.0 , 78.79 ± 3.9 , and $8.2 \pm 1.4 \Omega \cdot \text{cm}$, respectively, indicating that the addition of DMSO can improve the electrical conductivity of PEDOT:PSS network, and the more DMSO is added, the better the conductivity is. Next, we studied the sensitivity of the temperature

sensor prepared by different volume ratios of PEDOT:PSS and DMSO. The sensitivity S of the resistive temperature sensor is defined as $S = \Delta R/(R_0 \times \Delta T)$, where R_0 is the initial value of resistance, ΔR is the relative resistance change, and ΔT is the relative temperature change. It is worth noting that before the sensitivity test, the bottom cellulose base paper side of the thermosensitive layer was covered by a layer of single-sided tape to simulate its state in a dual-parameter tactile sensor. Fig. 2(b) shows the curves of relative resistance versus temperature of the thermosensitive sensors prepared with different volume ratios of PEDOT:PSS and DMSO. Between 25 $^{\circ}\text{C}$ and 65 $^{\circ}\text{C}$, the relative resistance change of PEDOT:PSS-based temperature sensor is negatively correlated with temperature change, and in the three temperature sensors studied, the lower the amount of DMSO added, the greater the negative correlation, indicating the higher sensitivity. Specifically, the sensitivities of the three sensors with PEDOT:PSS and DMSO volume ratios of 10:1, 20:1, and 40:1 are $-0.79 \text{ } ^{\circ}\text{C}^{-1}$, $-1.03 \text{ } ^{\circ}\text{C}^{-1}$, and $-1.71 \text{ } ^{\circ}\text{C}^{-1}$, respectively. The reason is that when the DMSO content is relatively low, the PEDOT:PSS molecular network will be more dispersed. After the temperature increases, the adhesion between the molecules in the PEDOT:PSS network increases rapidly, and the resistance decreases obviously, which is manifested as increased sensitivity. Next, the effect of water content on the sensitivity of temperature sensor with a PEDOT:PSS and DMSO volume ratio of 40:1 is studied. Fig. S8 in the Supporting Information shows that after a certain amount of deionized water ($V_{\text{DMSO}} : V_{\text{H}_2\text{O}} = 1:0, 1:1, 1:2$, and $1:5$) was added to the above thermosensitive ink, the initial resistivity of the thermosensitive layer made of this ink increases with the increase of water content, and the more water content in

the thermosensitive ink, the larger the initial resistance and relative resistance fluctuate with temperature (the test was repeated three times), resulting in an unstable performance [see Fig. 2(c)]. In view of the above results, the thermosensitive layer is prepared from the ink with PEDOT:PSS to DMSO volume ratio of 40:1 and additional deionized water.

Parameter optimization experiments for pressure-sensitive layer preparation were performed, and the average results of five tests were reported here. A series of pressure-sensitive layers were prepared by immersing dust-free wipes in 4%, 6%, 8%, and 10% aqueous dispersions of MWCNTs. Fig. 2(d) shows that the concentration of MWCNTs has a significant effect on the responsiveness of the pressure-sensitive layer. When the concentration of the MWCNTs decreases from 10% to 8% or even 6% in weight, the normalized resistance changes more obviously with pressure ($-0.34\% \text{ kPa}^{-1}$ for 10 wt.%, $-0.47\% \text{ kPa}^{-1}$ for 8 wt.%, and $-0.41\% \text{ kPa}^{-1}$ for 6 wt.%), but the linear relationship between the two becomes worse and worse. When we continued to reduce the MWCNTs concentration to 4 wt.%, the linearity is good at 0.993, but the sensitivity of the pressure-sensitive sensor decreases to $-0.39\% \text{ kPa}^{-1}$. To investigate the effect of immersing time on the performance of the pressure-sensitive sensor, we next soaked the dust-free wipe in 6 wt.% MWCNTs water dispersion for 0.5, 1, and 2 s. As can be seen from Fig. 2(e) and (f), there is a little difference in the initial conductivity and sensitivity of pressure-sensitive layers prepared by different immersion times. This is because of the strong water absorption of dust-free wipes, and the soaking process can be completed in a very short immersing time. Therefore, in the subsequent experiments, all pressure-sensitive layers would be prepared by immersing the dust-free wipe in 6 wt.% MWCNTs water dispersion for 1 s.

C. Sensing Performance and Characteristics of the VSDPS

Fig. 3(a) shows that the VSDPS can respond well to different magnitude pressures with high signal stability. In the pressure range of 0–45 kPa, the sensitivity reaches $-0.69\% \text{ kPa}^{-1}$, and the linearity is 0.9914. In the pressure range of 45–100 kPa, the pressure sensitivity is $-0.24\% \text{ kPa}^{-1}$, and the linearity is 0.9904 [see Fig. 3(b)]. Moreover, the VSDPS exhibits excellent responsiveness [see Fig. 3(c)]; when a pressure of 20 kPa was applied to the sensor, the response time and recovery time were 140 and 100 ms, respectively. At the same time, the VSDPS also shows good temperature response properties. Fig. 3(d) shows that when the VSDPS was transferred from room temperature to a high-temperature oven, the resistance of the thermosensitive component decreased responsively, and the greater the temperature difference, the more pronounced the decrease. When the VSDPS was transferred from the high-temperature oven back to room temperature, the resistance of the thermosensitive component returned to near its initial value. Fig. 3(e) shows that the VSDPS exhibits good sensitivity ($-1.71\% \text{ }^{\circ}\text{C}^{-1}$) and linearity (0.9893) to temperature changes in the range of 25 °C–65 °C. Also, it only takes 3 s to make a fast electrical signal response to the temperature change from 26 °C to 36 °C [see Fig. 3(f)]. In addition, the VSDPS exhibits good stability in both pressure

and temperature sensing modes. After 5000 pressure loading-releasing cyclic experiments between 0 and 40 kPa, the initial resistance of the pressure-sensitive component of the VSDPS only decreases by 1.8% [see Fig. 3(g)]. Also, the thermosensitive properties of the sensor hardly change during 50 cycles of heating-cooling experiments between 26 °C and 36 °C [see Fig. 3(h)], and the change range is consistent with the corresponding values in the sensitivity curve. In addition, we also compare the sensitivity of the VSDPS to temperature and pressure to other reported sensors [8], [11], [25], [26], [27]. Fig. S9 in the Supporting Information shows that the sensitivity of VSDPS to both temperature and pressure is comparable to state-of-the-art dual-parameter sensors with a similar temperature-sensitive range but a wider pressure response range. More importantly, as shown in Fig. S10 in the Supporting Information, ten of the prepared VSDPSs were randomly selected as test samples to investigate their two-parameter response characteristics. Between 0 and 30 kPa, the pressure sensitivity of the sensor slightly fluctuates around 0.69% ($0.69\% \pm 0.05\% \text{ kPa}^{-1}$), while between 25 °C and 65 °C, the temperature sensitivity fluctuates around 1.70% ($1.70\% \pm 0.1\% \text{ }^{\circ}\text{C}^{-1}$), which fully indicates that the VSDPS is reproducible.

To examine the signal crosstalk of the VSDPS, we first applied a pressure of 0–100 kPa to the VSDPS at a constant ambient temperature of 26 °C while recording the resistance change of the thermosensitive component of the sensor and plotted the average results of five tests in Fig. 4(a). Obviously, although the nominated resistance of the thermosensitive component fluctuates slightly in the $\Delta R/R_0$ versus pressure curve, its fluctuation range is in the order of 10^{-3} (0.13%), which is within the error range. These results fully demonstrate that the applied pressure has no effect on the electrical signal output of the thermosensitive component in the VSDPS. Meanwhile, another series of experiments were conducted to investigate the effect of temperature on the pressure-sensitive properties of the VSDPS. During experiments, the VSDPS was subjected to different pressures from a high-temperature object of 65 °C and compared it with the electrical signal response of the same pressure from a room-temperature object of 26 °C. The results in Fig. 4(b) shows that, under each pressure, the difference in the response signal due to the different temperature of the contact object is very small (the absolute value is less than 0.348%), especially compared to the resistance change caused by the pressure, it is not worth mentioning. When a single pressure of 10, 50, and 100 kPa was applied to the VSDPS at 26 °C, the relative resistance change rates of the pressure-sensitive component were as high as -6.87% , -33.53% , and -45.81% , respectively [see Fig. 3(b)]; however, the changes in normalized resistance caused by high temperature under the same pressure were only -0.297 , -0.095 , and -0.087 . The above results prove that the use of a 200-μm-thick insulating layer in our proposed VSDPS can effectively prevent the heat from spreading to its underneath pressure-sensitive layer and successfully avoid the signal crosstalk between the two sensitive components. It is worth noting that the above conclusions are based on the condition that the high temperature is derived from a contact object with a small area (not larger than the

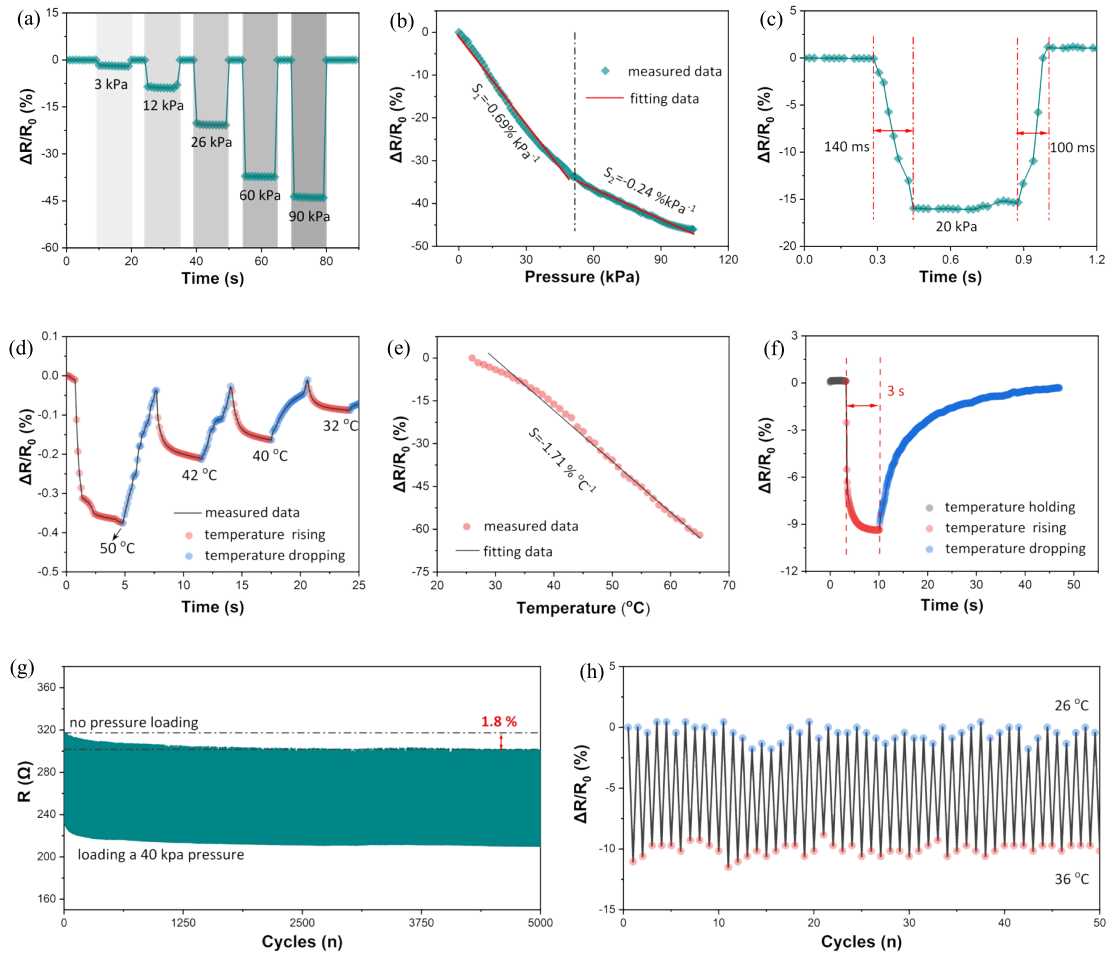


Fig. 3. Performance of the VSDPS in pressure and temperature sensing. (a) Change of normalized resistance of the VSDPS to different pressures. (b) Sensitivity determination curve of the sensor to pressure. (c) Response time of the VSDPS to loading and withdraw of a 20-kPa pressure. (d) Real-time response of the sensor to different temperatures. (e) Sensitivity determination curve of the sensor to temperature. (f) Response time of the VSDPS to temperature change. Cyclic experiments verifying the sensor's stability in response to (g) pressure and (h) temperature.

upper surface of the sensor) and does not apply to the overall heating of the environment, which will cause the pressure-sensitive component to be heated from all sides, eventually leading to design failure of the insulating layer.

Next, to verify the practicability of VSDPS, we performed mouth exhalation, finger press, and pulse monitoring tests on the sensor. Since the temperature of human exhaled air is usually higher than room temperature, when the tester exhaled to the sensor through the mouth at a distance of 10 cm, the thermosensitive component of the sensor immediately responded with an electrical signal reduced (the normalized resistance reduced by about 3.2%), and within 6-s continuous exhaling, the electrical signal remained constant [see Fig. 4(c)]. Once expiration stopped, the response signal quickly returned to its initial value. At the same time, the pressure-sensitive component did not make any signal changes because the impact force of the exhalation from the mouth to the sensor was too small. The results for the finger press test in Fig. 4(d) show that as the finger slowly approached the sensor from 5 cm away (this approaching progress took about 3 s), the resistance of the thermosensitive component gradually decreased. Until the contact press occurred, the

bimodal signals of temperature and pressure responded rapidly to a drop. Also, when the finger moved away, the pressure-sensitive signal quickly returned to the initial value, while the thermosensitive signal did not return to its initial value until the additional heat dissipated. The finger press test demonstrates that the VSDPS can also be used to detect the approach and departure of objects with a temperature difference from the sensor. Next, we arranged the sensor at the wrist for human temperature and pulse monitoring. Fig. 4(e) shows that, in a quiet state, the subject's body temperature is constant at 36.2 °C, and the heart rate is ~65 beats min⁻¹. Also, both the bimodal signals of temperature and pressure exhibit good stability, verifying the application potential of the VSDPS in the field of smart wearable devices.

III. APPLICATIONS

The above research shows that the VSDPS prepared by us can be used as a tactile sensor to sense the temperature of the contact object and the pressure exerted on the sensor, and the sensing signal is accurate and reliable. Therefore, based on the VSDPS, we constructed a flexible artificial sensory nervous system that mimics the biological tactile sensory system

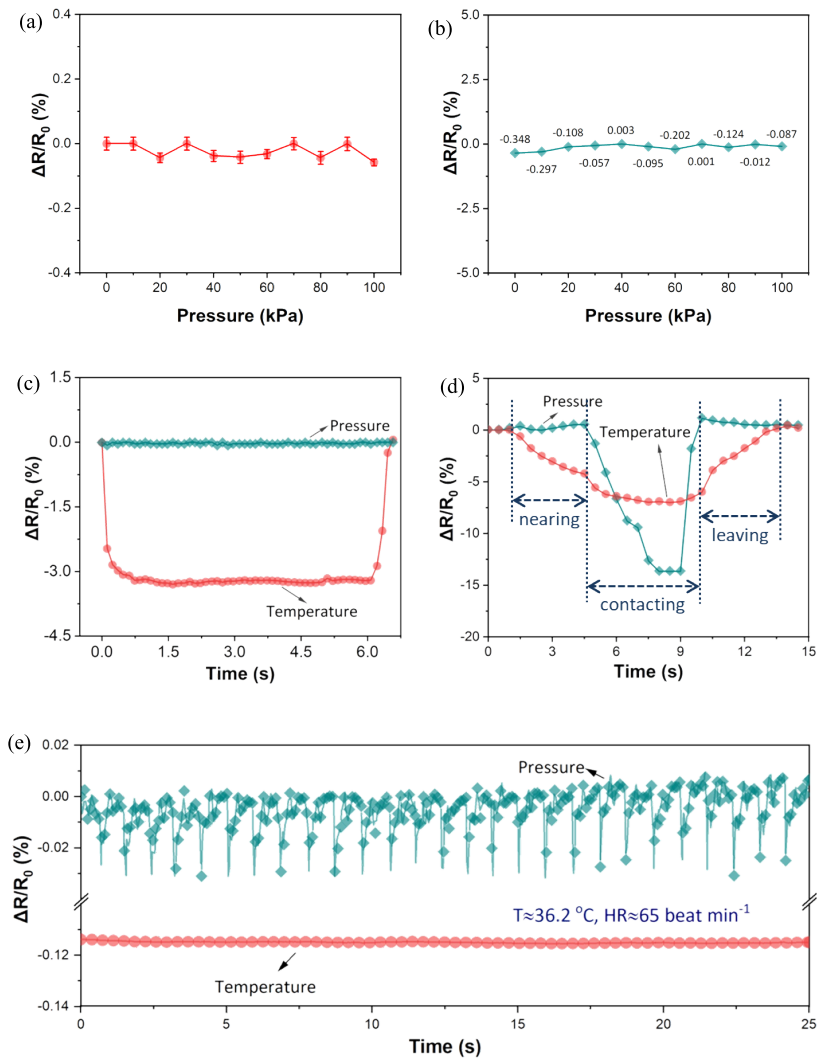


Fig. 4. Antisignal crosstalk performances of the VSDPS. (a) Normalized resistance of the thermosensitive component in a VSDPS when bearing different pressure at 26 °C. (b) Difference in normalized resistance of pressure sensing components when two objects with different temperatures 26 °C and 65 °C apply the same pressure to the VSDPS. Real-time response of dual-parameter sensor for (c) exhalation, (d) finger touch, and (e) wrist pulse and simultaneously body human temperature monitoring.

toward neuromorphic tactile recognition [see Fig. 5(a)]. In this system, tactile signals coded as spike trains are processed by synaptic devices with sensory memory, and tactile recognitions are achieved in a real-time and near-sensor manner by directly using device output without relying on computing resources or algorithms. We placed the sensor on the mechanical gripper of the robotic arm to simulate how the human body perceives external information as it touches an external object [see Fig. 5(b)]. Sensory neurons in the human skin provide a simple, intuitive interface that converts external temperature changes and skin contact information into physiological signals, which are then transmitted by central neurons to the cerebral cortex for information processing for touch recognition and brain learning. The dual-parameter sensor converts the external temperature and pressure information into a resistance change signal, which is converted into an independent analog signal by a single-chip microcomputer, and finally transmitted to a computer for environmental information analysis, which

is used by the machine gripper to sense external conditions. By cooperating with sensors, simulated artificial skin sensory neurons are constructed, which endow the robotic gripper with functions similar to human arms. The sampling frequency of the system is 1 kHz. Also, its dynamic range for pressure detection is from 0 to 100 kPa with a resolution of 0.4 kPa. Meanwhile, the dynamic range of the system for temperature detection is from 25 °C to 65 °C with a resolution of 0.5 °C. Fig. 5(c)–(e) shows that after being equipped with the flexible artificial sensory nervous system, when the mechanical gripper grabs normal-temperature objects, the temperature response curve remains constant, and the pressure response curve can real-time reflect the pressure it endures when grabbing objects of different weights.

Next, we control this mechanical gripper to grab the same glass bottle at different temperatures. Since the same object was grasped in the three grasping tasks as shown in Fig. 5(f)–(h), the pressure response curves showed nearly

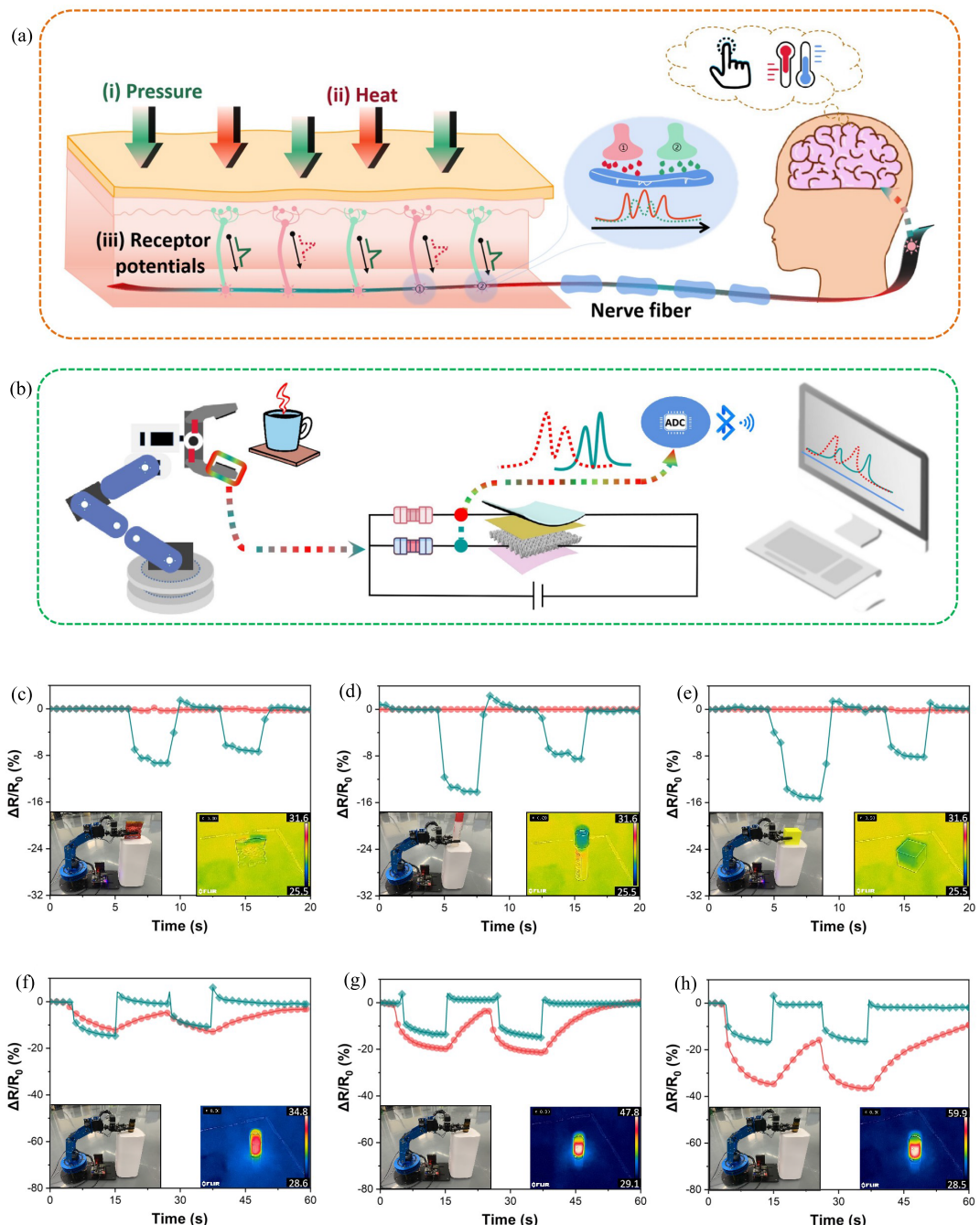


Fig. 5. Construction and application of flexible artificial sensory nervous system. (a) Functional diagram of biological sensory neurons, in which contact stimulation and temperature change stimulation are converted into different receptor potentials by skin layer receptors, and then, the receptor potential is induced by synapses to produce postsynaptic potentials, which are finally transmitted to the cerebral cortex through central neurons for information processing. (b) Schematic of the flexible artificial sensory nervous system. Dual-parameter sensing of temperature and pressure when mechanical gripper grabbing (c) bag of tea, (d) bottle of glue, and (e) cube with normal temperature. Dual-parameter sensing of temperature and pressure when mechanical gripper grabbing a glass bottle with a center temperature of (f) 34.8 °C, (g) 47.8 °C, and (h) 59.9 °C.

the same degree of variation. Meanwhile, the higher the temperature of the glass bottle, the more obvious the change of the temperature response curve. In addition, we also designed a designed mobile application to facilitate the application of the flexible artificial sensory nervous system (Video S1 in the Supporting Information). All the above applications show that the prepared dual-parameter sensor is able to accurately detect and distinguish between temperature and pressure, which presents

promising application prospects in robotics, human–machine interface, and smart wearable devices.

IV. CONCLUSION

In summary, based on a vertical stacking of sensing components strategy, we developed a dual-parameter sensor for pressure and temperature detection. The use of a thick double-sided tape between the pressure- and thermal-sensitive

components can effectively isolate electrical and thermal transfer between the two components, allowing the tactile inputs of pressure and temperature to be successfully differentiated without signal decoupling. The porous flexible photopaper substrate for thermosensitive component and the inherently compressible fabric substrate for pressure-sensitive component endow the VSDPS with good sensing performance in terms of sensitivity, response time, detection range, and stability for both pressure and temperature detection. The use of dispensing printing technology and immersion-drying process makes the preparation of the whole sensor simple and convenient for mass production. Since both pressure and temperature detection are based on the principle of resistance change, there is no need to apply bias voltage during the test, and the requirements for signal readout equipment are low. Based on above, a flexible artificial sensory nervous system was developed, which can help the robotic gripper to identify the weight and temperature of the grasped objects by directly using a self-written mobile application, verifying its application prospects in the field of intelligent interaction.

V. MATERIALS AND METHODS

A. Experimental Materials

PEDOT:PSS (1.5 wt.%, Clevios,¹ Germany), DMSO (Tianjin Zhiyuan Chemical Reagent Company Ltd.), silver paste (SCP003, Electrolube, Leicestershire, U.K.), and MWCNTs water dispersion (10 wt.%, XFWPMC-M33, Xianfeng Nano Company Ltd.) were used in the initial state without further purification.

B. Sensor Preparation

The sensors were prepared in layers and then integrated vertically, and its specific preparation process is schematically shown in Fig. S11 in the Supporting Information. First, a certain amount of PEDOT:PSS solution and DMSO were mixed in a volume ratio of 40:1. Next, by inkjet printing with a dispensing method, the mixture forms a pattern on the cellulose paper side of the photopaper by a microelectronic printer (Shanghai Power Electronics Technology Company Ltd., scientific 3A electronic printer). After drying and connecting the external electrode copper wire, the temperature-sensitive component was obtained. Meanwhile, the MWCNT/textile pressure-sensitive component was prepared by dipping double-knit wipe into MWCNTs water solution at room temperature for 1 s and then drying at 75 °C for 30 min. Finally, the 3M double-sided tape (0.5 mm thick) was clamped between the obtained pressure-sensitive and thermosensitive layers (note: the cellulose base paper side of the thermosensitive layer was placed facing the 3M tape), and the other side of the pressure-sensitive layer was encapsulated with a single-sided tape (0.15 mm thick) to cover the back encapsulation layer.

C. Sensing Performance Determination

Since the dual-parameter tactile sensor we developed with a vertical stacking structure is to give the robot human-like tactile perception, it is necessary to put the pressure

sensor to the robot and the temperature sensor to the external environment during use to sense the temperature and contact pressure of the contact object at the same time. Therefore, in all subsequent experiments, the thermosensitive layer side of the VSDPS is set as the outer contact surface to investigate the dual-parameter sensing characteristics. The tests to determine the sensitivity and response time of the VSDPS to pressure were carried out at 26 °C. A sensor is a device that converts external stimuli into electrical signals. However, in dual-parameter sensors, the electrical signals generated by different stimuli tend to crosstalk with each other, making the detection results unable to accurately quantify each external stimulus. Therefore, it becomes particularly meaningful to develop dual-parameter or even multimodal sensors without signal crosstalk. To examine the signal crosstalk of the VSDPS, we first applied a pressure of 0–100 kPa to the VSDPS at a constant ambient temperature of 26 °C while recording the resistance change of the thermosensitive component of the sensor, and the average results of five tests were reported here. Meanwhile, another series of experiments were conducted to investigate the effect of temperature on the pressure-sensitive properties of the VSDPS. It is conceivable that the higher the temperature of the contact object, the greater the impact on the responsive signal of the carbon material-based pressure sensing component, so we next tested the electrical signal response of the pressure-sensitive component when the VSDPS was subjected to different pressures from a high-temperature object of 65 °C and compared it with the electrical signal response of the same pressure from a room-temperature object of 26 °C. The experiment was repeated four times, and the difference in responsive signal measured at the same pressure but from the contact objects with different temperatures is plotted.

D. Characterization

Optical topography of the thermosensitive layer, pressure-sensitive layer, and cross section of the dual-parameter sensor was performed using an OLYMPUS-SZX10 microscope (Shanghai Puhe Optoelectronic Technology Company Ltd.). The temperature-sensitive properties of the VSDPS were determined by a thermosensitive testing system, which includes a DZF-6050 vacuum drying oven (Shanghai Jinghong Experimental Equipment Company Ltd.), a DMM6500 digital multimeter (KEITHLEY), and a JET-601 thermocouple thermometer. Before test, a thermocouple probe was pasted onto the outer surface of the VSDPS, and then, the VSDPS was connected to the DMM6500 multimeter using a double-wire resistance measurement mode. During the test, the resistance of the sensor was recorded in real time as temperature rising. The measurement frequency was 1 kHz and the tested temperature ranged from 26 °C to 65 °C. The pressure sensing performance of the VSDPS was determined by a universal testing machine (Suzhou Fuwenke Technology Company Ltd.) and a DMM6500 digital multimeter with a measurement frequency of 1 kHz and a tested pressure range within 0–100 kPa.

APPENDIX

Schematic and scanning electric microscope (SEM) images of the resin-coated photopaper, optical image of the

¹Trademarked.

thermosensitive component and the thermosensitive layer, SEM images of the pressure-sensitive layer, thermal isolation experiment, initial resistivity of the thermosensitive layer, sensitivity comparison, and schematic of the preparation process.

REFERENCES

- [1] H. Niu et al., "Perception-to-cognition tactile sensing based on artificial-intelligence-motivated human full-skin bionic electronic skin," *Adv. Mater.*, vol. 34, no. 31, Aug. 2022, Art. no. 2202622.
- [2] M. Zhu, J. Li, J. Yu, Z. Li, and B. Ding, "Superstable and intrinsically self-healing fibrous membrane with bionic confined protective structure for breathable electronic skin," *Angew. Chem.*, vol. 134, no. 22, May 2022, Art. no. e202200226.
- [3] H. Zhang, J. Guo, Y. Wang, L. Sun, and Y. Zhao, "Stretchable and conductive composite structural color hydrogel films as bionic electronic skins," *Adv. Sci.*, vol. 8, no. 20, Oct. 2021, Art. no. 2102156.
- [4] R. S. Johansson and A. B. Vallbo, "Tactile sensibility in the human hand: Relative and absolute densities of four types of mechanoreceptive units in glabrous skin," *J. Physiol.*, vol. 286, no. 1, pp. 283–300, Jan. 1979.
- [5] S. Zhao and R. Zhu, "Electronic skin with multifunction sensors based on thermosensation," *Adv. Mater.*, vol. 29, no. 15, Apr. 2017, Art. no. 1606151.
- [6] Y. Kumaresan, O. Ozioko, and R. Dahiya, "Multifunctional electronic skin with a stack of temperature and pressure sensor arrays," *IEEE Sensors J.*, vol. 21, no. 23, pp. 26243–26251, Dec. 2021.
- [7] W. Chunyu, "An all-silk-derived dual-parameter E-skin for simultaneous temperature-pressure detection," *ACS Appl. Mater. Interfaces*, vol. 9, pp. 39484–39492, Nov. 2017.
- [8] G. Y. Bae et al., "Pressure/temperature sensing bimodal electronic skin with stimulus discriminability and linear sensitivity," *Adv. Mater.*, vol. 30, no. 43, Oct. 2018, Art. no. 1803388.
- [9] J. C. Yang et al., "Microstructured porous pyramid-based ultrahigh sensitive pressure sensor insensitive to strain and temperature," *ACS Appl. Mater. Interfaces*, vol. 11, no. 21, pp. 19472–19480, May 2019.
- [10] S. Walia, I. Mondal, and G. U. Kulkarni, "Patterned Cu-mesh-based transparent and wearable touch panel for tactile, proximity, pressure, and temperature sensing," *ACS Appl. Electron. Mater.*, vol. 1, no. 8, pp. 1597–1604, Aug. 2019.
- [11] R. Wu et al., "Silk composite electronic textile sensor for high space precision 2D combo temperature-pressure sensing," *Small*, vol. 15, no. 31, Aug. 2019, Art. no. 1901558.
- [12] F. Zhang, Y. Zang, D. Huang, C.-A. Di, and D. Zhu, "Flexible and self-powered temperature-pressure dual-parameter sensors using microstructure-frame-supported organic thermoelectric materials," *Nature Commun.*, vol. 6, no. 1, pp. 1–10, Sep. 2015.
- [13] Y. Wang, H. Wu, L. Xu, H. Zhang, Y. Yang, and Z. L. Wang, "Hierarchically patterned self-powered sensors for multifunctional tactile sensing," *Sci. Adv.*, vol. 6, no. 34, Aug. 2020, Art. no. eabb9083.
- [14] F. Li et al., "Printable and stretchable temperature-strain dual-sensing nanocomposite with high sensitivity and perfect stimulus discriminability," *Nano Lett.*, vol. 20, no. 8, pp. 6176–6184, Aug. 2020.
- [15] J.-H. Lee et al., "Flexible temperature sensors made of aligned electro-spun carbon nanofiber films with outstanding sensitivity and selectivity towards temperature," *Mater. Horizons*, vol. 8, no. 5, pp. 1488–1498, May 2021.
- [16] S. Han, F. Jiao, Z. U. Khan, J. Edberg, S. Fabiano, and X. Crispin, "Thermoelectric polymer aerogels for pressure-temperature sensing applications," *Adv. Funct. Mater.*, vol. 27, no. 44, Nov. 2017, Art. no. 1703549.
- [17] Y.-E. Shin, S.-D. Sohn, H. Han, Y. Park, H.-J. Shin, and H. Ko, "Self-powered triboelectric/pyroelectric multimodal sensors with enhanced performances and decoupled multiple stimuli," *Nano Energy*, vol. 72, Jun. 2020, Art. no. 104671.
- [18] N. Trifigny, F. Kelly, C. Cochrane, F. Boussu, V. Koncar, and D. Soulard, "PEDOT: PSS-based piezo-resistive sensors applied to reinforcement glass fibres for in situ measurement during the composite material weaving process," *Sensors*, vol. 13, no. 8, pp. 10749–10764, Aug. 2013.
- [19] J. Rivnay et al., "Structural control of mixed ionic and electronic transport in conducting polymers," *Nature Commun.*, vol. 7, no. 1, pp. 1–9, Apr. 2016.
- [20] F. Jonas and W. Kraft, "New polythiophene dispersions, their preparation and their use," U.S. Patent 0440957 B1, Mar. 27, 1996.
- [21] D. Huang et al., "Perovskite solar cells with a DMSO-treated PEDOT: PSS hole transport layer exhibit higher photovoltaic performance and enhanced durability," *Nanoscale*, vol. 9, no. 12, pp. 4236–4243, 2017.
- [22] H.-S. Park, S.-J. Ko, J.-S. Park, J. Y. Kim, and H.-K. Song, "Redox-active charge carriers of conducting polymers as a tuner of conductivity and its potential window," *Sci. Rep.*, vol. 3, no. 1, pp. 1–6, Aug. 2013.
- [23] O. P. Dimitriev, D. A. Grinko, Y. V. Noskov, N. A. Ogurcov, and A. A. Pud, "PEDOT: PSS films—Effect of organic solvent additives and annealing on the film conductivity," *Synth. Met.*, vol. 159, nos. 21–22, pp. 2237–2239, Nov. 2009.
- [24] J. W. Xiang and E. Perzon, "Infrared photocurrent spectral response from plastic solar cell with low-band-gap polyfluorene and fullerene derivative," *Appl. Phys. Lett.*, vol. 85, pp. 5081–5087, Nov. 2004.
- [25] B. Liang et al., "Direct stamping multifunctional tactile sensor for pressure and temperature sensing," *Nano Res.*, vol. 15, no. 4, pp. 3614–3620, Apr. 2022.
- [26] Z. Gao, Z. Lou, W. Han, and G. A. Shen, "Self-healable bifunctional electronic skin," *ACS Appl. Mater. Interfaces*, vol. 12, no. 21, pp. 24339–24347, 2020.
- [27] J. Lee et al., "Rational design of all resistive multifunctional sensors with stimulus discriminability," *Adv. Funct. Mater.*, vol. 32, no. 1, Jan. 2022, Art. no. 2107570.